УДК 52-854, 523
DOI: 10.12737/szf-73202101

Поступила в редакцию 06.04.2021
Принята к публикации 07.06.2021

МОДЕЛИРОВАНИЕ ВИЗУАЛИЗАЦИИ МОНИТОРИНГА ЭНЕРГИЧНЫХ НЕЙТРАЛЬНЫХ АТОМОВ ГЕОМАГНИТОСФЕРЫ НА ЛУННОЙ БАЗЕ

SIMULATION STUDY OF THE ENERGETIC NEUTRAL ATOM (ENA) IMAGING MONITORING OF THE GEOMAGNETOSPHERE ON A LUNAR BASE

Ли Лу
Лаборатория исследования космического пространства, Национальный центр космических наук КАН, Пекин, Китай, luli@nssc.ac.cn
Пекинская главная лаборатория исследования космического пространства, Пекин, Китай
Главная научно-техническая лаборатория ситуационной осведомленности о космическом пространстве КАН, Пекин, Китай

Цин-Лун Ю
Лаборатория исследования космического пространства, Национальный центр космических наук КАН, Пекин, Китай, Yql04@nssc.ac.cn
Пекинская главная лаборатория исследования космического пространства, Пекин, Китай
Главная научно-техническая лаборатория ситуационной осведомленности о космическом пространстве КАН, Пекин, Китай

Пин Чжоу
Лаборатория исследования космического пространства, Национальный центр космических наук КАН, Пекин, Китай, pzhou@nssc.ac.cn
Пекинская главная лаборатория исследования космического пространства, Пекин, Китай
Главная научно-техническая лаборатория ситуационной осведомленности о космическом пространстве КАН, Пекин, Китай

Синь Чжан
Лаборатория исследования космического пространства, Национальный центр космических наук КАН, Пекин, Китай, xinchang@nssc.ac.cn
Пекинская главная лаборатория исследования космического пространства, Пекин, Китай
Главная научно-техническая лаборатория ситуационной осведомленности о космическом пространстве КАН, Пекин, Китай

Сянь-Го Чжан
Лаборатория исследования космического пространства, Национальный центр космических наук КАН, Пекин, Китай, changxg@nssc.ac.cn
Пекинская главная лаборатория исследования космического пространства, Пекин, Китай
Главная научно-техническая лаборатория ситуационной осведомленности о космическом пространстве КАН, Пекин, Китай

Li Lu
Laboratory of Space Environment Exploration, National Space Science Center of the Chinese Academy of Sciences, Beijing, China, luli@nssc.ac.cn
Beijing Key Laboratory of Space Environment Exploration, Beijing, China
Key Laboratory of Science and Technology on Space Environment Situational Awareness CAS, Beijing, China

Qing-Long Yu
Laboratory of Space Environment Exploration, National Space Science Center of the Chinese Academy of Sciences, Beijing, China, Yql04@nssc.ac.cn
Beijing Key Laboratory of Space Environment Exploration, Beijing, China
Key Laboratory of Science and Technology on Space Environment Situational Awareness CAS, Beijing, China

Ping Zhou
Laboratory of Space Environment Exploration, National Space Science Center of the Chinese Academy of Sciences, Beijing, China, pzhou@nssc.ac.cn
Beijing Key Laboratory of Space Environment Exploration, Beijing, China
Key Laboratory of Science and Technology on Space Environment Situational Awareness CAS, Beijing, China

Xin Zhang
Laboratory of Space Environment Exploration, National Space Science Center of the Chinese Academy of Sciences, Beijing, China, xinchang@nssc.ac.cn
Beijing Key Laboratory of Space Environment Exploration, Beijing, China
Key Laboratory of Science and Technology on Space Environment Situational Awareness CAS, Beijing, China

Xian-Guo Zhang
Laboratory of Space Environment Exploration, National Space Science Center of the Chinese Academy of Sciences, Beijing, China, changxg@nssc.ac.cn
Beijing Key Laboratory of Space Environment Exploration, Beijing, China
Key Laboratory of Science and Technology on Space Environment Situational Awareness CAS, Beijing, China

Синь-Юэ Ван
Лаборатория исследования космического пространства, Национальный центр космических наук КАН, Пекин, Китай, orchard@nssc.ac.cn
Пекинская главная лаборатория исследования космического пространства, Пекин, Китай
Главная научно-техническая лаборатория ситуационной осведомленности о космическом пространстве КАН, Пекин, Китай

Юань Чан
Лаборатория исследования космического пространства, Национальный центр космических наук КАН, Пекин, Китай, changyuan17@mails.ucas.ac.cn
Пекинская главная лаборатория исследования космического пространства, Пекин, Китай
Главная научно-техническая лаборатория ситуационной осведомленности о космическом пространстве КАН, Пекин, Китай
Университет КАН, Пекин, Китай

Xin-Yue Wang
Laboratory of Space Environment Exploration, National Space Science Center of the Chinese Academy of Sciences, Beijing, China, orchard@nssc.ac.cn
Beijing Key Laboratory of Space Environment Exploration, Beijing, China
Key Laboratory of Science and Technology on Space Environment Situational Awareness CAS, Beijing, China

Yuan Chang
Laboratory of Space Environment Exploration, National Space Science Center of the Chinese Academy of Sciences, Beijing, China, changyuan17@mails.ucas.ac.cn
Beijing Key Laboratory of Space Environment Exploration, Beijing, China
Key Laboratory of Science and Technology on Space Environment Situational Awareness CAS, Beijing, China
University of Chinese Academy of Sciences, Beijing, China

Аннотация. Поскольку время полного оборота Луны вокруг Земли в точности совпадает с периодом ее вращения вокруг своей оси, мы можем видеть только одну сторону Луны, обращенную к Земле. Благодаря отсутствию на Луне собственного корпускулярного излучения, на ее поверхности, обращенной к Земле, может быть установлена базовая станция телеметрии нейтральных атомов для осуществления долгосрочного непрерывного мониторинга геомагнитной активности. Разрабатывается двумерная система получения изображения энергичных нейтральных атомов (ЭНА) с полем зрения 20°×20°, угловым разрешением 0.5°×0.5° и геометрическим фактором ~0.17 см^2 ср. Моделирование магнитосферного кольцевого тока в энергетическом канале 4–20 кэВ для средней геомагнитной бури (K_p = 5) показывает следующее: 1) примерно на 60 R_E (R_E — радиус Земли) система получения изображения может получить 10^4 событий ЭНА за 3 мин, что соответствует статистическим требованиям к инверсии 2D кодированных данных изображений и удовлетворяет требованиям анализа эволюции кольцевого тока суббури во время магнитных бурь над средой; 2) загадки радиационных потерь ЭНА в областях магнитопаузы и плазменного слоя хвоста магнитосферы были выявлены с помощью двумерной модели излучения ЭНА. Мониторинг с высоким пространственно-временным разрешением изображений ЭНА этих двух важных областей обеспечит основу измерений поступления и механизма генерации энергии солнечного ветра; 3) средний интервал между регистрациями событий ЭНА составляет около 16 мс на орбите Луны; спектральная разница во времени для установленного диапазона энергий составляет минуты, что позволит получить информацию о местоположении для отслеживания триггера вспышек частиц во время геомагнитных бурь.

Abstract. Since the moon's revolution cycle is exactly the same as its rotation cycle, we can only see the moon always facing Earth in the same direction. Based on the clean particle radiation environment of the moon, a neutral atomic telemetry base station could be established on the lunar surface facing Earth to realize long-term continuous geomagnetic activity monitoring. Using the 20°×20° field of view, the 0.5°×0.5° angle resolution, and the ~0.17 cm^2 sr geometric factor, a two-dimensional ENA imager is being designed. The magnetospheric ring current simulation at a 4–20 keV energy channel for a medium geomagnetic storm (K_p=5) shows the following: 1) at ~60 R_E (R_E is the Earth radius), the imager can collect 10^4 ENA events for 3 min to meet the statistical requirements for 2D coded imaging data inversion, so as to meet requirements for the analysis of the substorm ring current evolution process of magnetic storms above medium; 2) the ENA radiation loss puzzles in the magnetopause and magnetotail plasma sheet regions have been deduced and revealed using the 2-D ENA emission model. High spatial-temporal resolution ENA imaging monitoring of these two important regions will provide the measurement basis for the solar wind energy input process and generation mechanism; 3) the average sampling interval of ENA particle events is about 16 ms at the moon's orbit; the spectral time difference for the set energy range is on the order of minutes, which can provide location information to track the trigger of geomagnetic storm particle events.

Keywords: energetic neutral atom (ENA), telemetry image, particle event, magnetosphere, ring current, magnetopause, plasma sheet.

Ключевые слова: энергичный нейтральный атом (ЭНА), телеметрическое изображение, вспышка частиц, магнитосфера, кольцевой ток, магнитопауза, плазменный слой.

INTRODUCTION

At present, our cognition of near-Earth space plasma originates mainly from in situ measurements of charged particles and electromagnetic fields, which give values of parameters at a given moment at a given point and do not provide an instantaneous overall picture of the phenomenon. It is a new development direction to obtain an instantaneous telemetry image of plasma in a large field of view in a specific state to understand the plasma distribution and evolution process throughout the magnetosphere.

Due to the resource constraints of satellites, most launched particle imaging satellites are equipped with one-dimensional detector arrays using satellite spin to collect two-dimensional ENA spatial distributions in exchange time for space, such as ASTRID/PIPPI [Barabash et al., 1997], IMAGE/H ENA [Burch, 2000], TC-2/NUADU [McKenna-Lawlor et al., 2004] TWINS [McComas et al., 2009], IBEX [McComas et al., 2011], etc. Two-dimensional ENA image signals of the magnetosphere are successfully obtained by satellite (such as IMAGE and TWINS) payloads in Earth's higher orbit; the globe energetic ion distribution of the magnetosphere is inversed according to the measurement image. However, due to the low time resolution (10–30 min) of the inversion results of relative geomagnetic activity time scale (e.g., ~30 min of substorm process), ENA imaging is in the research stage of energetic ion distribution pattern in geomagnetic space. It has not been really used for dynamic process analysis of geomagnetic activity. The present inversion results with the highest time resolution (~1 min) are derived from TC-2/NUADU [Lu et al., 2019] and are applied to the causal sequence analysis of particle events and environmental disturbances during geomagnetic activity. By comparing 4 min time resolution ENA image sequence with LANL's in situ measurements, Lu et al. [2016] have found that ring current energetic ions increase before ion injection from the magnetotail, which challenges the existing concept that ring current particles are injected earthward from the magnetotail.

At a higher lunar resonance orbit (apogee of $50R_E$), IBEX [McComas et al., 2011] also detects ENA emission signals from the magnetopause, polar cusp, and magnetotail. ENA integral images over 40 hrs provide large-scale magnetospheric particle distribution morphologies. It also includes a plasma sheet truncation in the magnetotail, or a similar plasmoid image. The duration of such events is usually of the order of tens of minutes, and their spatial form cannot be maintained for nearly 40 hrs.

For a spin satellite with one-dimensional detector array:

$$\text{the integral time of per pixel} =$$

$$= \text{scanning period } (s) \times \text{azimuth resolution } (°) / 360°.$$

For example, a two-dimensional detector array in a high orbit can improve the scanning integration time resolution of 0.5° azimuth resolution by 720 times, i.e., the scanning integration of the same counting ENA image in 40 hrs can be completed by the two-dimensional detector array in only 200 s. Developing a neutral atomic imager for two-dimensional detection array is therefore an effective way to improve payload time resolution.

The moon's period of revolution is exactly the same as its rotation period, so we see the moon always facing Earth in the same direction. Consider the clean particle radiation environment of the moon to establish a neutral atomic imaging telemetry base station on the lunar surface facing Earth, to develop a two-dimensional neutral atom imager with a small field of view (20°×20°), and to improve the spatial resolution of payload detection images by two-dimensional coding modulation design to realize long-term uninterrupted geomagnetic monitoring of Earth.

1. SCIENTIFIC OBJECTIVES

For the lunar outer space exploration environment, a neutral atom imager will carry on the global imaging measurement of Earth's magnetosphere. We study the overall structure and dynamics of the magnetosphere, as well as the influence and interaction of the magnetosphere with the solar wind and Earth's atmosphere. A global assessment of the magnetospheric structure and dynamics is expected to be made including: 1) probe objects: magnetospheric ring currents and plasmoid; 2) morphological changes of the magnetosphere: distortion of the magnetic field; 3) kinetic processes: magnetic storms or the trigger position and injection boundary of particle events during substorms.

Energetic ions in the magnetosphere are bound by the magnetic field in two forms: 1. Energetic ions in the ring current of the magnetosphere spiral around the magnetic field line at different pitch angles, and rebound between the north and south poles. After their charge exchange with the environmental neutral atoms evaporating from the upper geocorona, they produce ENA. Those ENAs containing information on the motion of energetic ions radiate omnidirectionally [Roelof, 1987; Goldstein, McComas, 2018]. A neutral atom imager can receive this ENA signal anywhere in space. 2. In the magnetopause or magnetotail plasma sheet region, most of the energetic ions trapped by the geomagnetic field have a 90° pitch angle. As the density of geocorona neutral atoms in the medium is low, the probability of generating ENA through the charge exchange is also low. But they only spread in the equatorial plane, and the flux decay is slow too. Neutral atom imagers in deep space can detect them only in the ecliptic plane.

The moon-based neutral atom imager will take ENAs of the ring current as the main detection object to create the simulation design for detection index analysis.

2. MOON-BASED ENA IMAGING MEASUREMENT SIMULATION

An average lunar orbit distance of 380000 km, ~60 Earth radii (R_E), 1 R_E with respect to the moon's

orbit has an angle of less than 1°. And the space range of the magnetospheres' ring current is between 2 and $8R_E$. The field of view of the instrument is therefore designed to be 20°×20°, and the angle resolution is better than 0.5°. It is planned to integrate 40 one-dimensional arrays each consisting of 40 detectors into a two-dimensional detector array. According to the lunar orbit (Figure 1, left) and a single detector's collimator (Figure 1, bottom), specific technical specifications of the simulation design of the lunar basic ENA imager are shown in Table 1. ENA generated by ring current energetic ions is the strongest omnidirectional emission source for particle imaging exploration of Earth's magnetosphere in lunar orbit. It is suitable for a tracer particle of ring current energetic ion distribution. The intensity and distribution of an ENA flux in different orbital positions are predicted by simulation, which is similar to the previous telemetry instrument design [Lu et al., 2014]. The simulation of ENA imaging was carried out in four positions in lunar orbit: new moon, first quarter, full moon, and last quarter (Figure 1, top). The hypothetical detector units as shown at the right of Figure 1 could be used to form a 40×40 2D detection array, with the center of the array pointing to Earth (the direction of the arrows at the four lunar positions at the left of Figure 1).

2.1. Imaging simulation of 2D ENA detector array

The ring current energetic ion flux distribution in the equatorial plane under geomagnetic activity index K_p=5 is shown in Figure 2 [Lu et al., 2020]. At a distance of $60R_E$, spatial resolution of the object is $0.526R_E$ (~3355 km) for 0.5° angle resolution. The simulation results of 3-min integral imaging for the ring current ENA emission source are presented in Figure 3.

While the details of the distribution of the ENA emission source of the ring current obtained at the 0.5° angle resolution are basically smoothed, the distribution profile of ENA emission distribution pattern of the magnetospheric ring current can still be given. Within the 20°×20° field of view, ~10^4 ENA events can be collected in 3 min, as shown in Table 2.

2.2 Imaging simulation of one-dimensional ENA detector array with a turntable scan

16 detector units (Figure 1, right) are arranged into a one-dimensional array of 8° elevation angles and added to a turntable scan of 360° azimuth angles. Select an azimuth resolution of 3° (~$0.1–0.42R_E$ corresponds to Earth); simulation ENA images and statistical ENA counts for 6 hr integration (the scan integration time per pixel is still 3 min) of the magnetospheric ring current are given in Figure 4 and Table 3 respectively.

We use inhomogeneous pixel grid points (elevation of ~3355 km, azimuth ~667–2669 km). The red region with a large flux in Figure 4 shows the basic characteristics of the low-altitude ENA emission source. However, because the minimum resolution distance in the elevation direction is relatively large, the ENA strong emission region is slightly amplified in this direction. The low-energy end of the ENA energy spectrum (4–20 keV) has been selected for imaging detection simulation. The

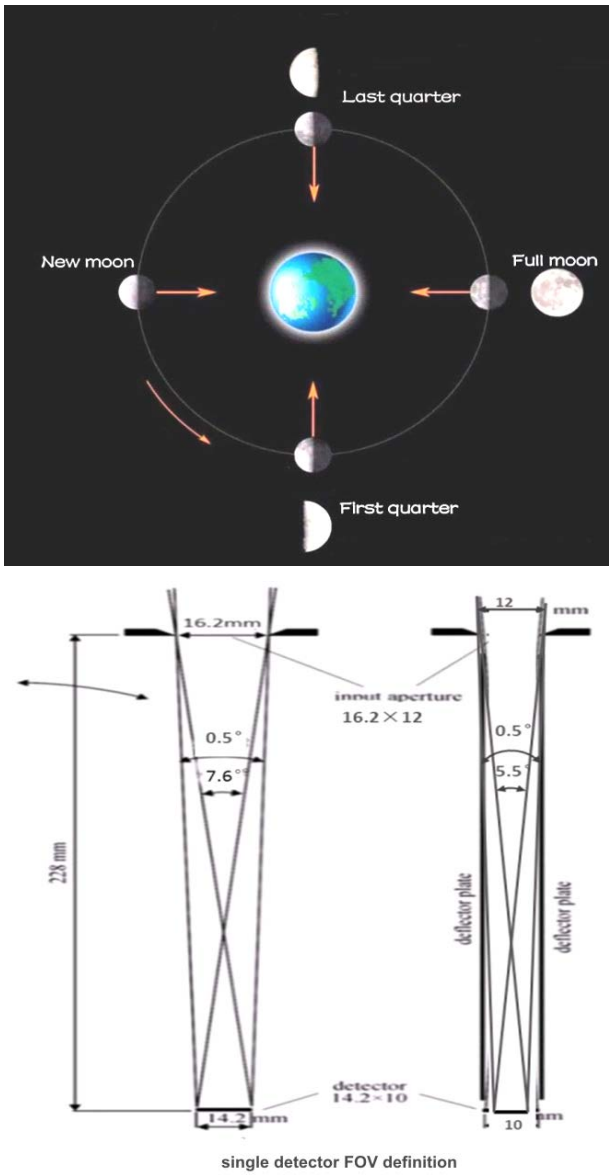

Figure 1. Schematic diagram of lunar orbit (top), geometry of single detector's collimator (bottom)

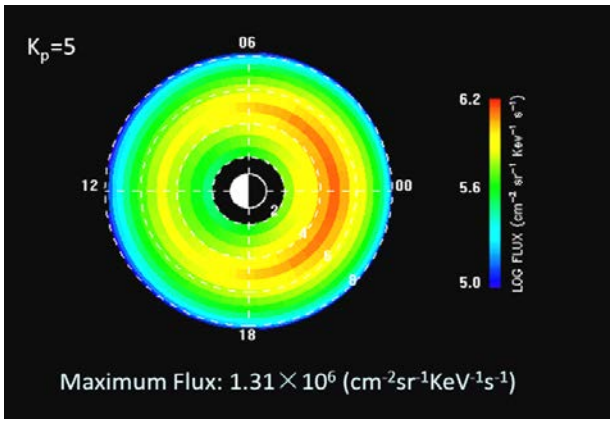

Figure 2. Model of equatorial energetic ion flux (4–20 keV) distribution of the magnetospheric ring current for a moderate magnetic storm (K_p=5)

blue coverage area with a lower ENA count in Figure 4 corresponds to the ENA emission directly through charge exchange in the region of the larger energetic ion flux of the ring current, which approximately circles the

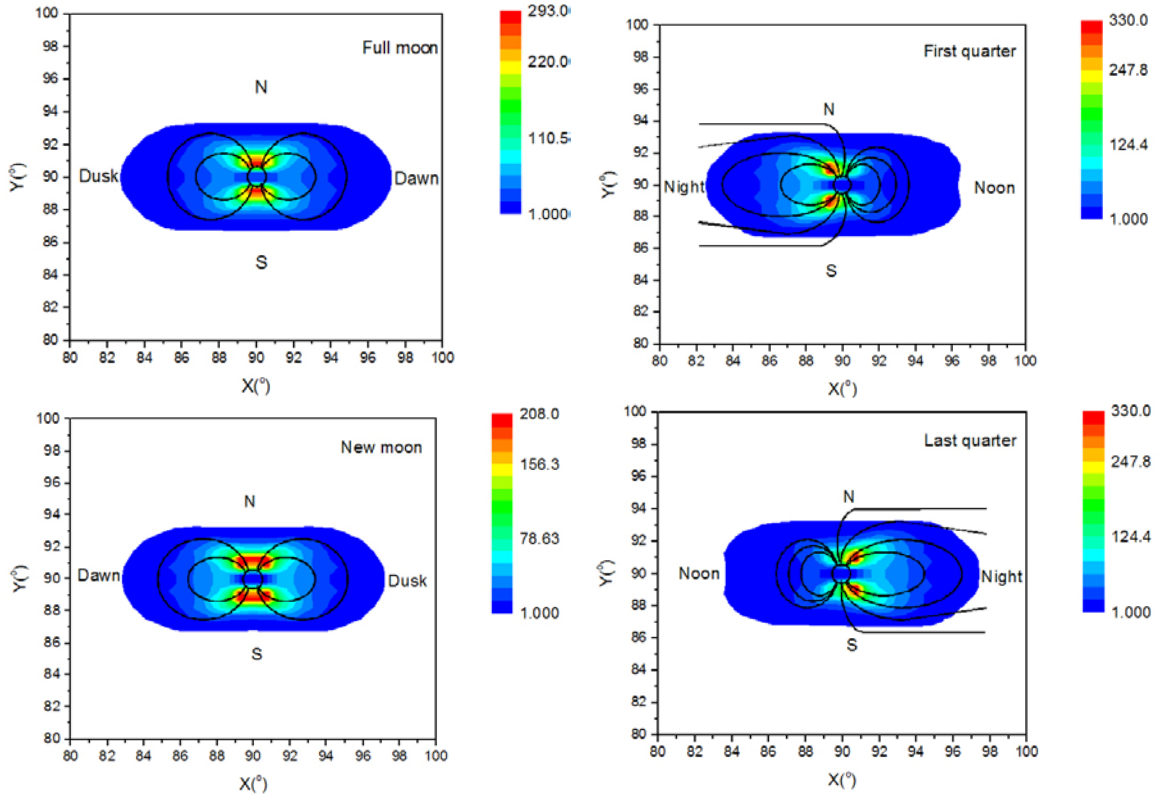

Figure 3. At the geomagnetic activity index K_p=5, simulation results with 3-min integrated imaging measurement of ENA emission sources of the ring current in four positions in lunar orbit: full moon (top left), first quarter (top right), new moon (bottom left), and last quarter (bottom right). Black curves are projections of geomagnetic field lines on each diagram respectively

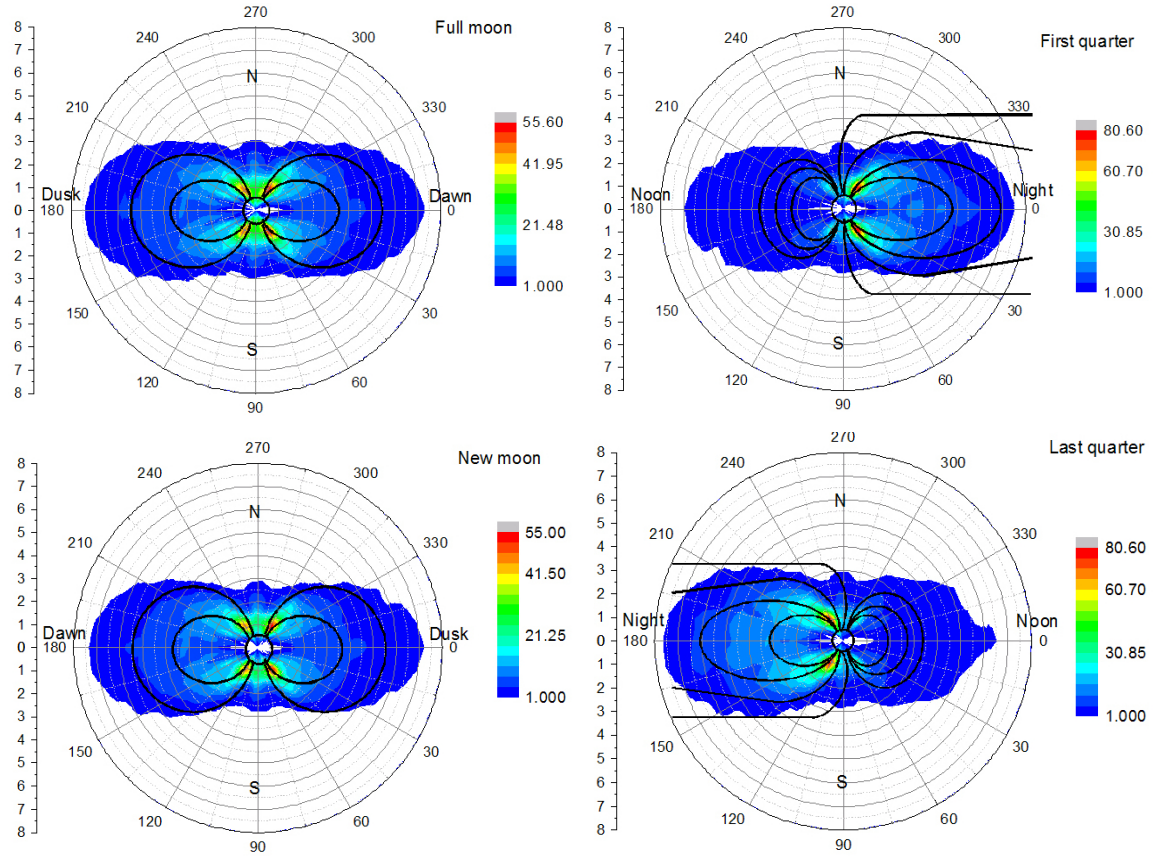

Figure 4. At the geomagnetic activity index K_p=5, simulation results with 6-hr scanning imaging of ENA emission sources of the ring current in four positions in lunar orbit: full moon (top left), first quarter (bottom right), new moon (bottom left), and last quarter (bottom right). Azimuth markings of FOV and the projection of magnetic field lines are added in the simulation diagrams

Table 1

Instrument simulation design parameters

Atomic species	H, O (simulation: H)
Energy range	4–200 keV (simulation: 4–20 keV)
Field of view	30°×30°(simulation: 20°×20°)
Angle resolution	≤0.5°(simulation: 0.5°×0.5°)
Geometric factor	Single detector: 10^{-4} cm^2sr; (simulation:×40×40≈0.173)
Sampling period	Simulation: 3 min
Element numbers	Simulation: 30 (latitude) × 60 (longitude) × 18 (L value) = 32400

Table 2

Statistics of ENA counts

	Average count	Maximum count	Total
Full Moon	6.8	297	10911
First quarter	6.4	334	10315
New Moon	5.9	213	9450
Last quarter	6.4	332	10309

Table 3

ENA counts

	Average count	Maximum count	Total
Full Moon	4.9	59	9597
First quarter	4.6	83	8911
New Moon	4.2	57	8199
Last quarter	4.6	82	8908

distribution range of Earth's magnetosphere. Due to the constraints of the geomagnetic field, the simulation images of the full moon (Figure 4, top left) and the new moon (Figure 4, bottom left) show the symmetrical ENA emission distribution characteristics of the flat circle, and the magnetotail distribution characteristics can be seen in the first quarter (Figure 4, top right) and the last quarter (Figure 4, bottom right).

3. MOON-BASED ENA IMAGING MEASUREMENT SCHEME AND RESULT EXPECTATION

3.1. 2D coded aperture modulation ENA imaging scheme

In view of the satellite resources, it is impossible to assemble 1600 detector units. The minimum time resolution of a one-dimensional array turntable with 16 detector units needs 6 hrs, which cannot meet the monitoring requirements of geomagnetic activity evolution. The simulation results show that the maximum sampling rate of an ENA event is about 60/s, the average sampling interval of particle event is more than 16 ms. Therefore, we propose to apply the technique used for gamma ray imaging [Goldwurm et al., 1999; Bassani et al., 2005] that involves using a two-dimensional coding aperture modulation technology to collect and transmit each single ENA event, $P_i(t, x, y, E)$. The ENA image will be retrieved afterwards with a decoding procedure. A 2D coded aperture modulation ENA imaging detector monomer structure, as shown in Figure 5, would consist of a 2D coded modulation grid (64×64 mm^2), collimator, starting carbon film, cutoff carbon film, MCP (80×80 mm^2) assembly, and 2D position sensitive readout electronics (50×50 grids). The technical parameters of the collimator of the 2D coded aperture modulation ENA imager (Table 4) are similar to those of the above 2D simulation array design.

Table 4

Technical parameters of collimator for 2D coded aperture modulation ENA imager

2D coding board modulation grid size	64×64 mm^2
Grid transmittance	50 %
2D position sensitive MCP size	80×80 mm^2
2D MCP reads out of grid points	50×50
Field of view	43°×43°
Angle resolution	0.5°×0.5°
Geometric factor	3.915 cm^2sr
High voltage deflector plate length	203 mm
High voltage deflector plate distance	80 mm

Tables 2 and 3 show that the maximum of 100 ENA counts can be obtained from the sampling integral results of a single pixel for 3 min, and the total ENA event count is close to 10^4, to meet the statistical requirements for the 2D coded modulation image inversion recovery. Here, the pixel distribution of the 2D inversion recovery image is continuous. The spatial resolution is only related to the ENA event statistics. The larger is the ENA event statistics, the higher is the spatial resolution of the 2D inversion recovery image.

3.2. Magnetospheric ring current monitoring

The main area of ENA event during geomagnetic activity is over the polar area of about 3000 km above the ground. The energetic ion flux up to 10^6 $cm^{-2}sr^{-1}keV^{-1}s^{-1}$ in the low-latitude region of $L=5$, the number of ENA events corresponding to pixels in the 3-min integration time is about a dozen. The ion flux around $L=8$ at the ring current is ~10^5 $cm^{-2}sr^{-1}keV^{-1}s^{-1}$ for the 3-min integration time, the ENA event count for pixels is only in the order of magnitude of the single digits, see Figures 2 and 3. The simulation does not consider the effect of noise, assuming that the particle emission environment is clean. During exploration, the single-digit particle count is submerged in noise, and the integration time of at least 2 orders of magnitude is added to obtain the effective recording of the contour shape of the magnetosphere, about 5 hr.

The general substorm disturbance period is more than 30 min. Simulation results show that the moon-based

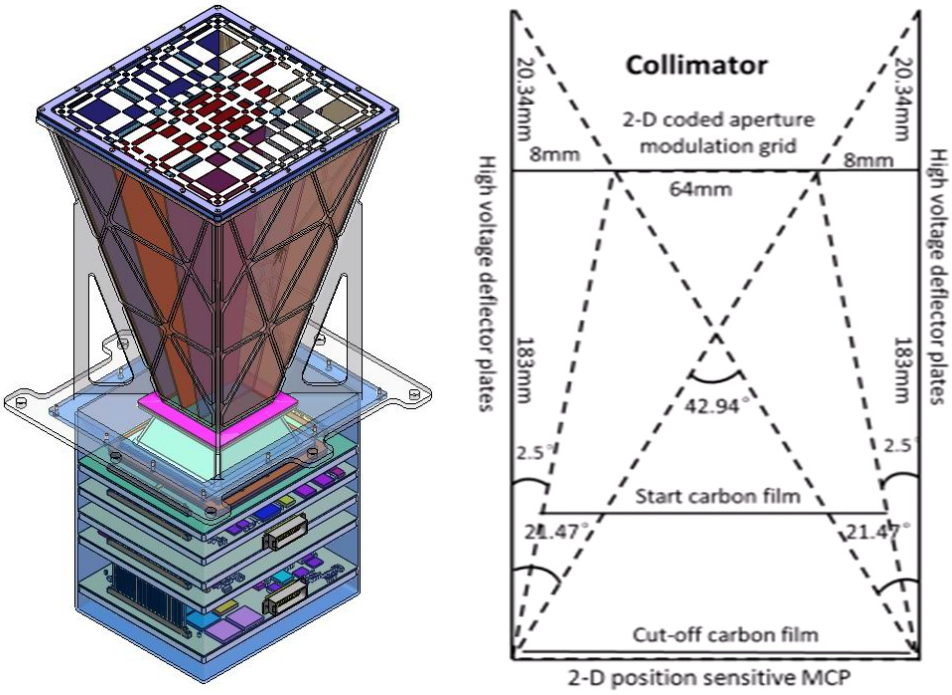

Figure 5. Schematic illustration of the 2D coded aperture modulated ENA detector (left) and geometry of the collimator (right)

ENA imager can retrieve the low height ENA signal distribution pattern reflecting the main characteristics of geomagnetic activity at a set time of 3 min, and meet the geomagnetic activity monitoring requirements.

3.3. ENA emission loss puzzles in the magnetopause and magnetotail plasma sheet regions

During the geomagnetic activity, the IBEX satellite simultaneously observed an ENA emission enhancement at the magnetopause and the polar cusp on the lunar resonance Orbit [IBEX Data Release 12, ORBIT 52, 2019] with about the same order of magnitude. ENA imagers on board the Earth-orbiting satellites had never measured a strong ENA flux signal from the magnetopause or from the plasma region. It is by at least two orders of magnitude weaker than the ENA emission signal generated by the ring current, in the cusp region. The measurement facts of the IBEX satellite in the lunar resonance orbit give rise to the puzzle of the missing ENA emission in the magnetopause and magnetotail plasma sheet regions.

At the magnetopause and in the plasma sheet of the magnetotail formed under the action of solar wind pressure, the pitch angle of the energetic ions picked up by the geomagnetic field is 90°. The background geocorona neutral atoms and their density distribution are inversely proportional to the square of the geocentric distance [Rairden et. al., 1983]. The ENA generated by the charge exchange of energetic ions and upper geocorona atoms can only propagate in the equatorial plane. Although the original ENA emission flux is small, the attenuation (inversely proportional to R_E) of 2D propagation is relatively low. At the magnetopause (about a dozen R_E), the density of low-energy neutral atoms evaporated from the geocorona deccreases to 10^{-2} of the cusp region, and there is no order-of-magnitude difference in energetic ion fluxes between the magnetopause and the cusp. In lunar resonance orbit ($50R_E$) or lunar orbit($60\ R_E$), in view of the conservation of total ENA emission flux, the ENA emission flux at the magnetopause and in the cusp decreases by R^{-1} and R^{-2} respectively, which are about 2×10–2 and 3×10–4 of the original ones. Generally, the orbit inclination of Earth's satellite that carried the ENA imager is larger, is not operating near the equatorial plane. The ENA emission flux from the magnetopause and plasma sheet is weak. So, the ENA Imager carried by Earth-orbiting satellites has never observed a clear ENA imaging of the magnetopause and the magnetotail plasma sheet. Just within the ecliptic plane near the moon, the omnidirectional ENA emission flux generated by the ring current achieves balance with the 2D ENA emission flux driven by the magnetopause and the magnetotail plasma sheet. The IBEX-HI's measurement in orbit 23 [McComas et al., 2011] illustrates just this point. Suspected plasma sheet truncation (10:48 UT on the 5th to 02:23 UT on the 7th November 2009, orbit 52) or the plasmoid (from 21:21 UT on the 27th to 13:40 UT on the 29th October 2009, orbit 51) was obtained by IBEX in lunar resonance orbit [McComas et al., 2011], but they can hardly last 40 hrs. The IBEX measurement (orbit 51) may be interpreted as the average image of multiple plasmoid events repeated for about 40 hrs during the magnetic storm. Imagine if we could complete the ENA emission distribution pattern imaging measurement of plasmoid for 3 min, it can be used as a direct detection basis for the plasmoid generated by magnetotail reconnection.

The magnetopause, the magnetotail plasma sheet, and the polar cusp are three important gateways for solar wind energy input to the magnetosphere. The distri-

bution pattern and evolution process of ENA emission in these regions can provide information on the solar wind energy input mechanism, and they are very important monitoring regions. Moon-based ENA imaging monitoring FOV can cover the entire magnetosphere, and simultaneously obtain ENA emission signals from these three important regions with basically balanced flux intensity. During the geomagnetic activity period, the distribution pattern, evolution process, and response time sequence of ENA emission of the magnetopause, ring current, and plasma sheet will provide an important basis for revealing the geomagnetic activity mechanism.

3.4. Particle trigger event tracing

The ENA imaging array is intended to use the 2D coded modulation energy spectrum recording, particle events with a temporal resolution of up to millisecond. For deep space exploration (~60R_E), the ENA spectral response of different energies in geomagnetic activity events has an about minute time difference (Table 5). It is assumed that different energetic ions produced by an acceleration mechanism (e.g., magnetic reconnection) are injected at the initial triggering site of geomagnetic activity simultaneously. From the response time difference between energy spectrum curves of different energy channels, the emission source location of energetic ions can be inferred: the less the time difference in the energy

Table 5

Energy and detection delay time of H ENA at 60 R_E distance

E (keV)	*T* (*s*)
5	392.31
10	277.46
100	87.732
1000	27.738

spectrum response, the shorter the transport distance of energetic ions causing the charge exchange. It is generally believed that there are two possible sources of energetic ions: one is the entry of energetic ions directly from the solar wind at polar cusps, and the other is the precipitating energetic ions accelerated along the magnetic field line from the magnetotail. The time difference in the ENA spectrum generated above can be calculated according to different propagation distances. We can use the detected ENA spectrum time difference containing the energetic ion motion information to track the trigger position generated by the energetic ion events [Lu et al., 2020].

When our payload is placed on the dark side of the moon, we can obtain an all-sky map of ENA flux distributions similar to the all-sky map of H differential flux detected by IBEX-Hi over the past three years [McComas et al., 2012]. By using the particle tracking technique mentioned above, we can estimate whether these ENA emission signals are from the heliopause or not. At the very least, the parallax of the ENA ribbons in different energy channels [McComas et al., 2012] provides information about the location of the ENA emission source.

SUMMARY

The moon has a clean radiation environment and a stable surface facing Earth. It is beneficial for the limited FOV ENA imager to target the ground, and suitable for the establishment of an ENA imaging monitoring station and a docking daily transit data transmission ground station. During the lunar day (from first quarter, full moon to the last quarter) charging phase, the payload around the magnetotail is convenient to monitor in the main energetic particle flux distribution and evolution of the ring current. At 60 R_E from Earth, in the ecliptic plane, the 2D ENA emission of the magnetopause and the magnetotail plasma sheet has fluxes with the same order of magnitude as the omnidirectional ENA emission generated by the ring current in the cusp region. The simulation results show that the minimum temporal resolution of ENA imaging is about 3 min, and the 2D spatial resolution is better than 0.5°×0.5°, which meets the needs of monitoring the distribution pattern and evolution of energetic particles in geomagnetic activities. Among them, the short timescale evolution of ENA emission patterns of the magnetopause and magnetotail plasma sheets is an important basis for revealing the energy process and transformation mechanism of geomagnetic activities. Energy spectrum recording mode of 2D coded modulation of ENA imager, $P_i(t, x, y, E)$ and the time difference in the ENA energy spectrum generated by 60 R_E distance transmission also provide indirect data support for geomagnetic activity trigger location tracking.

This study was supported by the Strategic Priority Program (SPP) on Space Science Advanced Research of Space Science Issues and Payloads (No. XDA 15017100).

REFERENCES

Bassani L., Rosa A.D., Bazzano A., Bird A.J., Dean A.J., Gehrels J.B., et al. Is the integral/ibis source IGR J17204-3554 a gamma-ray-emitting galaxy hidden behind the molecular cloud NGC 6334. *Astrophys. J.* 2005, vol. 634, L21. DOI: 10.1086/498718.

Barabash S., C:son Brandt P., Norberg O., Lundin R., Roelof E.C., Chase C.J., et al. Energetic neutral atom imaging by the ASTRID microsatellite. *Adv. Space Res.* 1997, vol. 20, no. 4-5, pp. 1055–1060.

Burch J.L. IMAGE mission overview. *Space Sci. Rev.* 2000, vol. 91, pp. 1–14. DOI: 10.1023/A:1005245323115.

Goldstein J., McComas D.J. The Big Picture: Imaging of the Global Geospace Environment by the TWINS Mission. *Rev. Geophys.* 2018, vol. 56, iss. 1, pp. 251–277. DOI: 10.1002/2017RG000583.

Goldwurm A., Goldoni P., Laurent P., Lebrun F. Imaging simulations of the galactic nucleus with the ibis gamma-ray telescope on board integral. *Astrophys. Lett. Communications*. 1999, vol. 38, pp. 333–336.

IBEX Data Release 12. Remote measurements of magnetospheric Energetic Neutral Emissions by the Interstellar Boundary Explorer, 2019. http://ibex.swri.edu/ibexpublicdata Data_Release_12.

Lu L., McKenna-Lawlor S, Balaz J., Shi Jiankui, Yang Chuibai, Luo Jing. Technical configuration and simulation of the NAIS-H for the MIT mission. *Chin. J. Space Sci.* 2014, vol. 34, iss. 3, pp. 341–351. DOI: 10.11728/cjss2014.03.341.

Lu L., McKenna-Lawlor S, Cao J B, Kudela K, Balaz J. The causal sequence investigation of the ring current ion-flux

increasing and the magnetotail ion injection during a major storm. *Science China Earth Sciences*. 2016, vol. 59, pp. 129–144. DOI: 10.1007/s11430-015-5121-7.

Lu L., McKenna-Lawlor S., Balaz J. Close up observation and inversion of low-altitude ENA emissions during a substorm event. *Science China Earth Sciences*. 2019, vol. 62, pp. 1024–1032. DOI: 10.1007/s11430-018-9307-x.

Lu L., Yu Q.-L., Lu Q. Near-approach imaging simulation of low-altitude ENA emissions by a LEO satellite. *Front. Astron. Space Sci*. 2020, vol. 7, id. 35. DOI: 10.3389/fspas.2020.00035.

McComas D.J., Allegrini F., Baldonado J., Blake B., Brandt P.C., Burch J., et al. The two wide-angle imaging neutral-atom spectrometers (TWINS) NASA mission-of-opportunity. *Space Sci. Rev*. 2009, vol. 142, pp. 157–231). DOI: 10.1007/s11214-008-9467-4.

McComas D.J., Carrico J.P., Hautamaki B., Intelisano M., Lebois R., Loucks M., et al. A new class of long-term stable lunar resonance orbits : Space weather applications and the Interstellar Boundary Explorer. *Space Weather*. 2011, vol. 9, iss. 11, S11002. DOI: 10.1029/2011SW000704.

McComas D.J., Dayeh M.A., Allegrini F., Bzowski M., de Majistre R., Fujiki K., et al. The frist three years of IBEX observations and our evolving heliosphere. *Astrophys. J. Supplement Series*. 2012, vol. 203, no. 1.

McKenna Lawlor S., Balaz J., Barabash S., Johnsson K., Lu L., Shen C., et al. The energetic NeUtral Atom Detector Unit (NUADU) for China's Double Star Mission and its Calibration. *Nuclear Inst. & Methods*. 2004, vol. 503, iss. 3, pp. 311–322. DOI: 10.1016/j.nima.2004.04.244.

Rairden R L, Frank L.A., Craven J.D. Geocoronal imaging with dynamics explorer. *Geophys. Res. Lett*. 1983, vol. 91, no. A12, pp. 13613–13630. DOI: 10.1029/GL010i007p00533.

Roelof E.C. Energetic neutral atom image of a storm-time ring current. *Geophys. Res. Lett*. 1987, vol. 14, iss. 6, pp. 652–655. DOI: 10.1029/GL014i006p00652.

How to cite this article:

Li Lu, Qing-long Yu, Ping Zhou, Xin Zhang, Xian-guo Zhang, Xin-yue Wang, Yuan Chang. Simulation study of the energetic neutral atom (ENA) imaging monitoring of the geomagnetosphere on a lunar base. *Solar-Terrestrial Physics*. 2021. Vol. 7. Iss. 3. P. 3–11. DOI: 10.12737/szf-73202101.